

A Linear Implementation of an Analog Resonate-and-Fire Neuron

Angqi Liu^{*1}, Filippo Moro^{*1}, Sebastian Billaudelle¹, Melika Payvand¹

¹*Institute of Neuroinformatics, University of Zurich and ETH Zurich, Zurich, Switzerland*

^{*}*Equal contribution*

Email: {filippo, angqi, sebastian, melika}@ini.uzh.ch

Abstract—Oscillatory dynamics have recently proven highly effective in machine learning (ML), particularly through State-Space Models (SSMs) that leverage structured linear recurrences for long-range temporal processing. Resonate-and-Fire (RAF) neurons capture such oscillatory behavior in a spiking framework, offering strong expressivity with sparse event-based communication. While early analog RAF circuits employed nonlinear coupling and suffered from process sensitivity, modern ML practice favors linear recurrence. In this work, we introduce a resonate-and-fire (RAF) neuron, built in 22 nm FDSOI technology, that aligns with SSM principles while retaining the efficiency of spike-based signaling. We analyze its dynamics, linearity, and resilience to Process–Voltage–Temperature (PVT) variations, and evaluate its power, performance, and area (PPA) trade-offs. We map the characteristics of our circuit into a system-level simulation where our RAF neuron is utilized in a keyword-spotting task, showing that its non-idealities do not hinder performance. Our results establish RAF neurons as robust, energy-efficient computational primitives for neuromorphic hardware.

Index Terms—Resonate-and-Fire Neuron, Analog State-Space Models

I. INTRODUCTION

Oscillatory dynamics have recently emerged as a powerful computational principle in machine learning [1, 2, 3, 4]. A central development in this direction has been SSM architectures [5, 6], which employ structured linear recurrences to capture long-range temporal dependencies with remarkable efficiency and scalability. By leveraging oscillatory latent dynamics, these models have demonstrated state-of-the-art performance on sequential tasks while maintaining robustness and favorable memory–computation trade-offs [1]. This progress highlights the role of oscillations not only in biological systems [7], but also in artificial architectures, where they act as compact and expressive primitives for temporal processing.

Introduced as a second-order extension of leaky-integrate-and-fire models, with only one state variable, the membrane state, RAF neurons naturally embody oscillatory dynamics, thanks to the coupling of two state variables in the spiking domain [8]. Such neurons exhibit damped subthreshold oscillations, coincidence detection, and frequency selectivity. These properties render them highly expressive units for neuromorphic computing, with temporal richness and event-driven communication. As such, they represent a biologically inspired, yet hardware-efficient bridge between the continuous

oscillations exploited in SSMs and the discrete signaling of spiking networks.

Early analog designs for RAF neurons relied on non-linearly coupling the two state variables, often inspired by Lotka–Volterra oscillator circuits [9, 10], to approximate the second-order dynamics of the RAF model. While effective in demonstrating resonant behavior, these analog realizations suffered from sensitivity to device mismatch, process variations, and temperature fluctuations. Importantly, they cannot directly model the SSM-like equations, due to the non-linear coupling of the states. More recently, digital implementations have been explored [11], motivated by their scalability, programmability, and resilience to PVT variations.

In this work, we revisit the RAF neuron through the lens of modern ML-driven, i.e. SSMs, design principles. Specifically, we introduce an analog electronics implementation of a RAF, based on 22 nm Fully-Depleted Silicon on Insulator (FDSOI) technology, shown in Fig. 1. We use Transconductance Amplifiers (TCAs) to linearly couple the two states of the neuron, and leverage Switched-Capacitor (SC) circuits for controlling the dynamics of each state (Fig. 1). Our design is energy efficient and the proposed RAF neuron consumes [1.6 - 132.6] nW depending on the desired resonance frequency, which is set by the TCA biasing current. We evaluate the linearity of the coupling by analyzing the TCA, as well as the range of the temporal dynamics provided by the SC circuit, and analyze the non-idealities introduced by our design. We propose to mitigate such non-idealities with a co-design approach where the circuit’s characteristics are accounted for in system-level simulation. We demonstrate the effectiveness of such an approach to solve a keyword spotting task in simulation.

II. FROM SSMs TO RAF NEURONS

SSMs have recently demonstrated remarkable capabilities in processing long temporal sequences [5, 1], owing to their structured linear recurrence that captures rich dynamics while remaining computationally efficient. The continuous-time SSM formulation can be written as $\dot{x}(t) = Ax(t) + Bu(t)$ and $z(t) = \sigma(Cx(t))$. A , B , and C are the system matrices governing the state transition and readout, σ a non-linear function.

The RAF neuron [8] can be viewed as a biologically inspired, energy-efficient distillation of the SSM model, embedding oscillatory state dynamics within a spiking framework.

The presented work has received funding from the Swiss National Science Foundation Starting Grant Project UNITE (TMSGI2-211461).

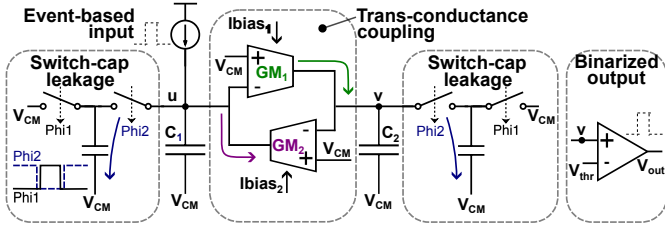


Fig. 1. Linear-Resonate-and-Fire block-level circuit diagram.

The RAF neuron simplifies the SSM equation by removing the C matrix projection and using a heaviside non-linearity for the output. Furthermore, the RAF model features a particular structure for the A transition matrix, leading to the following continuous-time form:

$$\begin{aligned} \dot{x}(t) &= A_{RAF} x(t) + B_{RAF} I(t) \\ &= \begin{bmatrix} -\frac{1}{\tau_u} & -\omega_v \\ \omega_u & -\frac{1}{\tau_v} \end{bmatrix} \begin{bmatrix} u(t) \\ v(t) \end{bmatrix} + \begin{bmatrix} 1 \\ 0 \end{bmatrix} \begin{bmatrix} I_u(t) \\ 0 \end{bmatrix} \\ z(t) &= \mathcal{H}(v(t) - \Theta) \end{aligned} \quad (1)$$

where u and v denote the two internal state variables (analogous to the real and imaginary parts of an SSM state x), $\tau_{u/v}$ is a time constant for either the u or v state, $\omega_{u/v}$ is the coupling factor between the neurons states, and proportional to the resonance frequency, $I(t)$ the input current. The neuron emits a spike when the state v reaches a threshold Θ , and we do not include a reset mechanism in the model. The circuit implementation of the Heaviside function is realized with a voltage comparator applied to the state v .

III. CIRCUIT IMPLEMENTATION

The proposed circuit realizes the RAF neuron described in Eq. (1), with emphasis on preserving the linearity of the state coupling coefficients. The two internal states, u and v , are represented by voltages stored on capacitors C_1 and C_2 , respectively. Their interaction follows a cross-coupling scheme mediated by a pair of linear TCA, while their intrinsic decay is implemented through programmable SC leakage paths. We propose the SC instead of a DC biased subthreshold transistor as in [12, 13] to reduce mismatch and maintain fidelity to the ideal exponential decay. Figure 1 illustrates the overall architecture of the RAF cell, highlighting its modular structure where oscillatory coupling and leakage are independently tunable. With reference to Eq. 1, the time constant is expressed as a function of the switching frequency f_{SC} : $\tau_{u,v} = 1/f_{SC}$. Note that the circuit allows for independent control of the time constant of states u and v via dedicated switching frequencies $f_{SC,u,v}$. The resonance frequency is instead proportional to the TCA's linear transconductance, $g_{m1,2}$, which in turn is a function of its biasing current, I_{bias} : $\omega_{u,v} = g(I_{bias}) \approx g_{m1,2}$.

A. Linear Transconductance Amplifier

The transconductance amplifiers implement the linear cross-coupling (coefficients $\omega_{u,v}$) between the two state variables

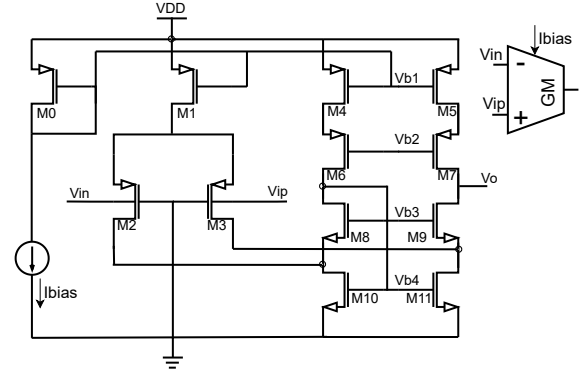


Fig. 2. GM stage implemented through a bulk-driven cascoded TCA

in Eq. (1). Each amplifier converts the voltage of one state into a current that charges or discharges the other state capacitor, thereby setting the resonance frequency ω . To ensure faithful reproduction of the linear SSM dynamics, the transconductance element must exhibit high linearity over the full oscillation voltage swing, typically from ground to V_{DD} .

Previous solutions for low-power, linear TCAs, such as in [14], employ a large ($M\Omega$ -range) tail resistance, which occupies a large area. In this work, this limitation is addressed by utilizing a cascoded bulk-driven differential pair [15], shown in Fig. 2. This topology is selected for its ability to provide low transconductance (g_m), high output impedance, and high linearity. Furthermore, the implementation in FDSOI technology is advantageous, as the bulk isolation can be more effectively realized.

As shown in Fig. 2, the amplifier's transconductance (g_m) is set by the input pair M2 and M3. This pair is biased by the tail current source M1, which mirrors the external reference current (I_{bias}) from M0. A cascode output stage (M4-M11) boosts the output impedance. Note that output impedance should be maximized to avoid non-ideal leakage from the states u and v through the TCA output stages. To ensure sufficient voltage headroom for oscillation, the output stage is biased using a standard wide-swing configuration [16].

The linearity of the proposed TCA circuit is evaluated under various biasing conditions, with results presented in Fig. 3. The design achieves a relatively linear output range spanning 0 V to 0.8 V, corresponding to the full dynamic range available for the states u and v as constrained by the power supply rails. The variance of the transconductance (g_m) is subsequently employed in system-level simulations to model the non-ideal linearity of the TCA.

Leveraging to the linearity of the TCAs, our proposed RAF neuron faithfully reproduces the behavior modeled by equation 1, as revealed by the circuit dynamics of the couple oscillator in Fig. 4. This behavior is obtained using $I_{bias} = 1$ pA and $f_{SC} = 10$ kHz. The oscillation envelope reveals a decay behavior, governed by the SC frequency (f_{SC}), in this case set to the same value for both states u and v . Furthermore,

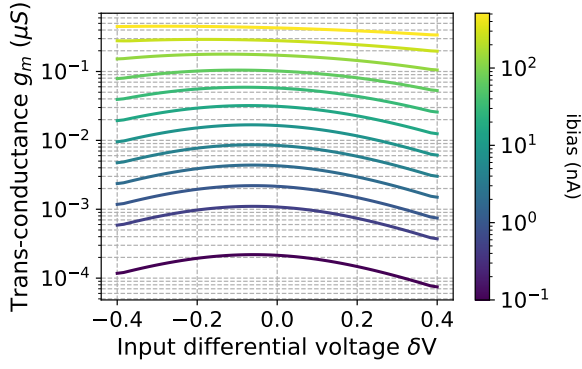


Fig. 3. Linearity of the bulk-driven TCA implementing the GM stage (Fig.2), under different I_{bias}

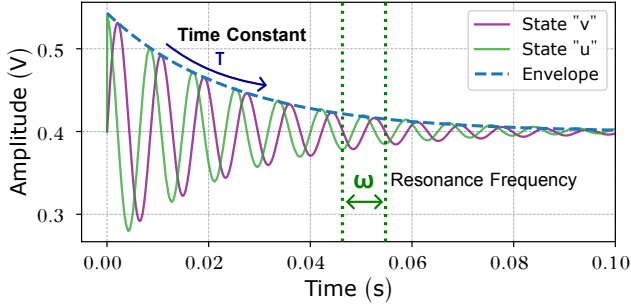


Fig. 4. Dynamics of the coupled oscillator of Fig. 1 with $I_{bias} = 1$ pA and $f_{SC} = 10$ kHz.

the resonance frequency ω is determined by the g_m provided by the TCA, which is tuned by the bias current I_{bias} . The coupled states u and v experience a 90° phase shift, and the decay aligns linearly with both the u and v signals.

As shown in Fig. 5, the resonance frequency scales with I_{bias} with a linear dependency, confirming that the oscillatory behavior can be adjusted through the current bias of the TCA. This design achieves both a large dynamic range of resonance frequencies and large output impedance, the latter being critical to minimize state-dependent leakage effects discussed later.

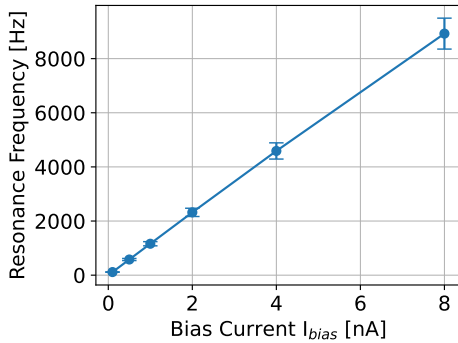


Fig. 5. Resonance frequency as a function of the TCA's bias current.

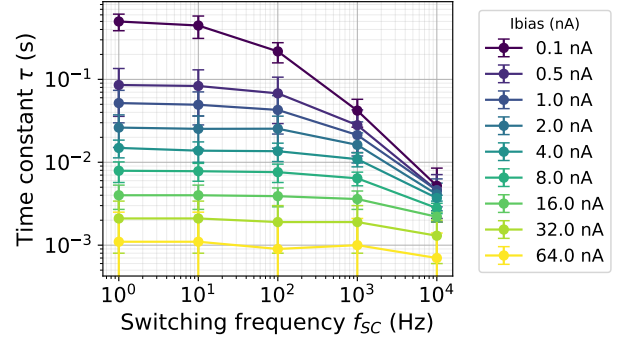


Fig. 6. Time constant for the two states u and v as a function of the switching frequency f_{SC} , and for different TCA bias currents I_{bias} .

B. Switched Capacitor exponential decay

The intrinsic decay terms of the RAF neuron, corresponding to the diagonal elements $\tau_{u,v}$ of the system matrix in Eq.1, are realized using SC circuits. Leveraging the low-leakage properties of FDSOI technology, the SC circuit can operate at a very low f_{SC} to achieve time constants on the order of hundreds of milli-seconds while consuming negligible power and occupying a small area. The SC structure periodically discharges the state capacitor to a virtual common-mode node, emulating a controllable resistive path with an equivalent conductance proportional to $C_{fringe} \cdot f_{SC} / C_{1,2}$, where f_{SC} is the switching frequency. Adjusting f_{SC} thus allows direct tuning of the neuronal time constants $\tau_{u,v}$.

Monte Carlo (MC) characterization of the circuit yields the programmable time constants reported in Fig. 6. The results show that the decay constants can be tuned over more than two orders of magnitude, approximately from 500 ms down to 1 ms, covering a dynamic range compatible with temporal processing in speech, biomedical, and robotic control applications. The analysis also reveals a secondary dependency of the time constant on the bias current I_{bias} of the transconductance stage that drives the same node. This coupling between I_{bias} and $\tau_{u,v}$ originates from finite output impedance of the TCA and is analyzed in the following subsection.

C. Limitations of this approach

Although the proposed design enforces linear state coupling, the finite output impedance of the transconductance amplifiers introduces an additional parasitic leakage path that modulates the effective time constant of each state. Consequently, the decay rates are not solely determined by the SC circuitry but also by the TCA's output impedance, set by its DC operating point. Higher I_{bias} values increase the transconductance and resonance frequency while reducing output resistance, leading to a saturation, or "clipping", of the maximum achievable $\tau_{u,v}$, as shown in Fig. 6.

We mitigate this effect through two complementary strategies. First, as already mentioned, the amplifier output stages adopt a cascoded topology to boost output impedance without sacrificing transconductance linearity. Second, at the system

level, we incorporate this non-ideality in a compact behavioral model of the RAF circuit, which is used in large-scale neuromorphic simulations to accurately capture the bias-dependent time-constant compression. This co-design approach ensures that algorithmic simulations and circuit-level performance remain consistent.

D. Summary of circuit performance

Table I summarizes the performance of the designed RAF. In contrast to previously proposed neurons [10], this design provides enhanced control over a broad range of time constants and intrinsic oscillation frequencies, with a tuning range sufficient for real-time signal processing applications.

The total power consumption of the RAF neuron is dominated by the static biasing of the transconductance amplifiers. Because the TCA is current-biased, its contribution scales approximately as $I_{\text{bias}} \cdot V_{\text{DD}}$, leading to an almost linear relationship between oscillation frequency and power. The SC section contributes only a small dynamic component proportional to f_{SC} , which remains nearly constant across our power estimation. As a result (Fig. 7), the total dynamic power grows proportionally with I_{bias} , with an empirical slope of 16.5 nW/nA. The reported range of 1.6–132.6 nW corresponds to $I_{\text{bias}} \in 0.1\text{--}8.0$ nA. The output comparator is not included in this estimate.

TABLE I
PERFORMANCE SUMMARY THE RAF CIRCUIT. *DEPENDING ON TCA
BIAS CURRENT AND REQUIRED RESONANCE FREQUENCY

Technology [nm]	22
Oscillation principle	Gm-C
Oscillator type	Harmonic
Supply voltage [V]	0.8
Power consumption [nW]	1.6 – 132.6*
Frequency range [Hz]	$100 - 500 \times 10^3$
Area [μm^2]	6524
Additional voltage regulator/ current reference required	NO/YES

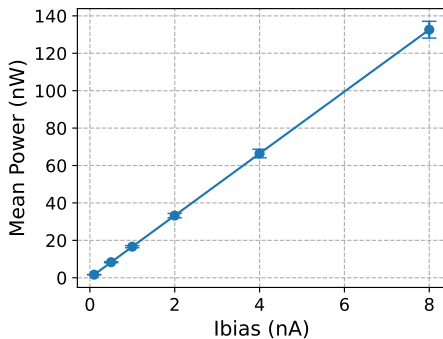


Fig. 7. Dynamic power consumption as a function of the bias current I_{bias}

IV. SYSTEM LEVEL SIMULATION OF THE LRAF CIRCUIT

To evaluate the computational capabilities of the proposed RAF circuit under realistic hardware constraints, we performed

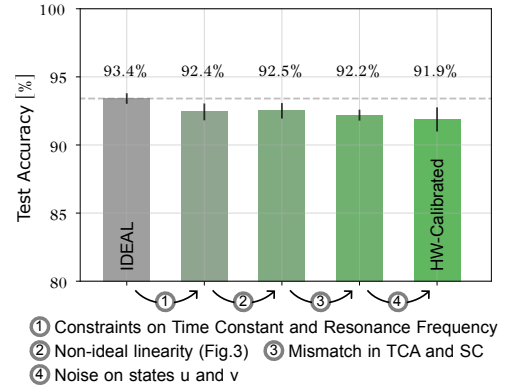


Fig. 8. Classification accuracy on the SHD task with different levels of hardware-awareness to the RAF circuit’s non idealities.

a system-level simulation on a keyword spotting task using the Spiking Heidelberg Digits (SHD) dataset. The experiments build upon the codebase in [3], adapted to match our RAF dynamics and parameterization. All simulations employ 8-bit quantized synaptic weights, reflecting the precision typically used in edge neuromorphic processors where memory footprint is a critical constraint.

We progressively introduce different degrees of hardware awareness into the neuron model to bridge the gap between the ideal mathematical formulation in Eq. (1) and simulation from the designed circuit. We estimated fixed-pattern deviations and temporal noise from Monte Carlo and transient noise simulations. Five levels of abstraction are defined. First, the Ideal model, which is the discretized version of the continuous-time RAF equations, without any hardware constraints. Progressively, we add: (1) Constraints on the resonance frequency ω and time constants $\tau_{u,v}$ according to Fig. 5 and Fig. 6; (2) Non-ideal linearity of the TCA according to Fig. 3; (3) Device Mismatch acting on the resonance frequency ω and time constants $\tau_{u,v}$ parameters; (4) Additive white noise on the states u and v , resulting in a complete hardware-calibrated behavioral model.

The classification results across these levels are summarized in Fig. 8, showing a small drop (1.5%) of classification accuracy from the ideal to the hardware aware level.

V. CONCLUSION

We present a RAF circuit that follows the recent oscillatory models in machine learning, such as SSMs, by implementing a linear two-state coupling. The circuit employs a bulk-driven transconductance amplifier and a switched-capacitor design, achieving both high linearity and time constants suitable for real-time signal processing. While intrinsic non-idealities introduce deviations from the ideal linear RAF behavior, their impact is mitigated through hardware-aware system-level simulations. In this work, we prove the efficacy of this co-design approach achieving competitive keyword spotting performance. Future work will be needed to extend the approach to different task domains.

REFERENCES

- [1] T Konstantin Rusch and Daniela Rus. “Oscillatory state-space models”. In: *arXiv [cs.LG]* (Oct. 2024).
- [2] Felix Effenberger et al. “The functional role of oscillatory dynamics in neocortical circuits: A computational perspective”. en. In: *Proc. Natl. Acad. Sci. U. S. A.* 122.4 (Jan. 2025), e2412830122.
- [3] Maximilian Baronig et al. “Advancing Spatio-Temporal Processing in Spiking Neural Networks through Adaptation”. In: *arXiv [cs.NE]* (Aug. 2024).
- [4] Maxime Fabre, Lyubov Dudchenko, and Emre Neftci. “Structured state space model dynamics and parametrization for spiking neural networks”. In: *arXiv [cs.NE]* (June 2025).
- [5] Albert Gu, Karan Goel, and Christopher Ré. “S4 - Efficiently Modeling Long Sequences with Structured State Spaces”. In: *arXiv [cs.LG]* (Oct. 2021).
- [6] Svea Marie Meyer et al. “A diagonal structured state space model on Loihi 2 for efficient streaming sequence processing”. In: *arXiv [cs.LG]* (Sept. 2024).
- [7] Olesia Dogonashcheva et al. “Rhythm-based hierarchical predictive computations support acoustic-semantic transformation in speech processing”. en. In: *Nat. Comput. Sci.* 5.10 (Oct. 2025), pp. 915–926.
- [8] Eugene M Izhikevich. “Resonate-and-fire neurons”. In: *Neural networks* 14.6-7 (2001), pp. 883–894.
- [9] Kazuki Nakada, Tetsuya Asai, and Hatsuo Hayashi. “Analog VLSI implementation of resonate-and-fire neuron”. In: *International Journal of Neural Systems* 16.6 (2006), pp. 445–456.
- [10] Kazuki Nakada, Tetsuya Asai, and Hatsuo Hayashi. “A silicon resonate-and-fire neuron based on the Volterra system”. In: *Proceedings of the International Symposium on Nonlinear Theory and its Applications (NOLTA)*. 2005, pp. 101–104.
- [11] Trung-Khanh Le, Trong-Tu Bui, and Duc-Hung Le. “Modeling and Designing of an All-Digital Resonate-and-Fire Neuron Circuit”. In: *IEEE Access* 11 (2023), pp. 62318–62334.
- [12] Arianna Rubino et al. “Ultra-low-power FDSOI neural circuits for extreme-edge neuromorphic intelligence”. In: *IEEE Transactions on Circuits and Systems I: Regular Papers* 68.1 (2020), pp. 45–56.
- [13] Giacomo Indiveri et al. “Neuromorphic silicon neuron circuits”. In: *Frontiers in neuroscience* 5 (2011), p. 73.
- [14] Sining Pan and Kofi A. A. Makinwa. “A 10 fJ·K² Wheatstone Bridge Temperature Sensor With a Tail-Resistor-Linearized OTA”. In: *IEEE Journal of Solid-State Circuits* 56.2 (2021), pp. 501–510. DOI: 10.1109/JSSC.2020.3018164.
- [15] Sebastian Billaudelle et al. “An accurate and flexible analog emulation of AdEx neuron dynamics in silicon”. In: *2022 29th IEEE International Conference on Electronics, Circuits and Systems (ICECS)*. 2022, pp. 1–4. DOI: 10.1109/ICECS202256217.2022.9971058.
- [16] E. Sackinger and W. Guggenbuhl. “A high-swing, high-impedance MOS cascode circuit”. In: *IEEE Journal of Solid-State Circuits* 25.1 (1990), pp. 289–298. DOI: 10.1109/4.50316.